INSTITUTE OF PHYSICS PUBLISHING PHYSICS IN MEDICINE AND BIOLOGY

Phys. Med. Biol. **49** (2004) 5295–5308 PII: S0031-9155(04)84030-2

Heat-transfer dynamics during cryogen spray cooling of substrate at different initial temperatures

Wangcun Jia[1], **Guillermo Aguilar**[1,2], **Guo-Xiang Wang**[3] **and J Stuart Nelson**[1]

[1] Beckman Laser Institute, University of California, 1002 Health Sciences Road East, Irvine, CA 92612-1475, USA
[2] Department of Mechanical Engineering, University of California, Riverside, CA 92521, USA
[3] Department of Mechanical Engineering, University of Akron, OH 44325, USA

E-mail: wjia@uci.edu

Received 27 July 2004, in final form 8 October 2004
Published 10 November 2004
Online at stacks.iop.org/PMB/49/5295
doi:10.1088/0031-9155/49/23/007

Abstract

Cryogen spray cooling (CSC) is used to minimize the risk of epidermal damage during laser dermatologic therapy. However, the dominant mechanisms of heat transfer during the transient cooling process are incompletely understood. The objective of this study is to elucidate the physics of CSC by measuring the effect of initial substrate temperature (T_0) on cooling dynamics. Cryogen was delivered by a straight-tube nozzle onto a skin phantom. A fast-response thermocouple was used to record the phantom temperature changes before, during and after the cryogen spray. Surface heat fluxes (q'') and heat-transfer coefficients (h) were computed using an inverse heat conduction algorithm. The maximum surface heat flux ($q''_{\max}$) was observed to increase with T_0. The surface temperature corresponding to $q''_{\max}$ also increased with T_0 but the latter has no significant effect on h. It is concluded that heat transfer between the cryogen spray and skin phantom remains in the nucleate boiling region even if T_0 is 80 °C.

(Some figures in this article are in colour only in the electronic version)

Nomenclature

A	area (m^2)
b	aluminium foil thickness (m)
C	specific heat (J (kg °C)$^{-1}$)
d	nozzle inner diameter (mm)
h	heat-transfer coefficient (W (m^2 °C)$^{-1}$)
l	nozzle length (mm)

k	thermal conductivity (W (m $^\circ$C)$^{-1}$)
q''	heat flux (W m^{-2})
T	temperature ($^\circ$C)
t	time (s or ms)
y	vertical coordinate (m)
z	nozzle-to-substrate distance (mm)

Greek symbols

α	thermal diffusivity (m^2 s^{-1})
Δt	cryogen spurt duration (ms)
ρ	density (kg m^{-3})
τ	response time (ms)

Subscripts

0	initial
Al	aluminium
crit	critical
c	cryogen
d	droplet
ec	effective cooling
L	liquid
Leid	Leidenfrost
max	maximum
min	minimum
N	nozzle
sat	saturation

1. Introduction

Ideal laser treatment of cutaneous vascular lesions requires selective thermal necrosis of blood vessels with minimal damage to the normal overlying epidermis and adjacent dermis (Anderson and Parrish 1983). However, non-specific absorption by epidermal melanin competes for absorption of laser radiation in subsurface target chromophores. If not controlled, high epidermal temperatures can lead to blistering, dyspigmentation or scarring, which limit the laser radiant exposure that can be safely applied. Pre-cooling of the epidermis with cryogen spurts permits the safe application of laser pulses with higher energy (Nelson *et al* 1995, 1996), leading to improved therapeutic outcome for port wine stains (PWS) (Nelson *et al* 1995, Waldorf *et al* 1997, Chang and Nelson 1999), haemangiomas (Chang *et al* 1998, 2001), rhytides (Kelly *et al* 1999) and hair removal (Nahm *et al* 2002). Despite the wide clinical use of cryogen spray cooling (CSC) and considerable research efforts in recent years, our understanding of the involved heat-transfer mechanisms and dynamics remains incompletely understood. It is therefore not certain whether existing CSC devices have been optimized for their respective clinical applications.

The main parameter that characterizes transient CSC is the surface heat flux (q'') through the skin. Previous studies to determine q'' during CSC have utilized epoxy blocks, metal disks and thin metal films with Plexiglas® substrates. Torres *et al* (1999) used an epoxy block embedded with thermocouples during CSC experiments and found the maximum surface heat flux ($q''_{\max}$) to be approximately 75 kW m^{-2}. Karapetian *et al* (2003) obtained a $q''_{\max}$ around 1100 kW m^{-2} for a $d_N = 0.57$ mm and $z = 25$ mm using a silver disk embedded in an epoxy

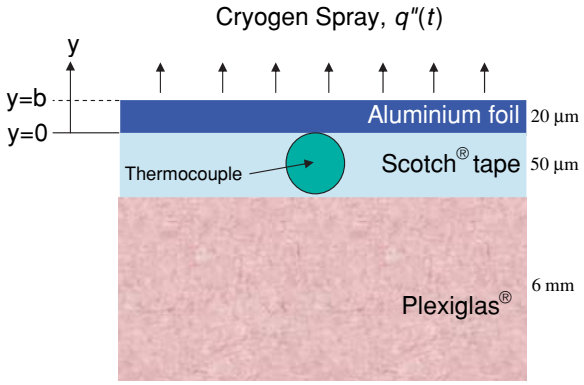

Figure 1. Model of one-dimensional inverse heat transfer (not to scale).

resin plate. Aguilar *et al* (2003b) carried out CSC experiments with a Plexiglas® substrate covered by aluminium foil and found q''_{max} was between 430 and 620 kW m^{-2} for $z = 50$ and 20 mm, respectively, and a d_N of 0.7 mm. It can be seen that the measured q'' for metal substrates is much higher than those of epoxy blocks or Plexiglas® substrates. Since the thermal properties of the epoxy or Plexiglas® resemble those of skin, those substrates are deemed more appropriate to study the effects of CSC on human tissue.

Aguilar *et al* (2002) numerically investigated the possibility of applying multiple-intermittent cryogen spurts and laser pulses to patients with darker skin types. The simulation indicates that this combination could, under certain conditions, permit the use of higher laser light doses while providing sufficient epidermal protection. The simulation also showed that the epidermis might attain a temperature of 80 °C at the end of laser exposure and immediately before a subsequent cryogen spurt. However, no data on the heat-transfer dynamics during CSC at such high surface temperature are available in the literature. As a result, constant heat-transfer coefficient (h) is used in all analyses regardless of surface temperature. Previous studies on water spray cooling of metal substrates have shown that h is dependent on surface temperature (Qiao and Chandra 1998, Ciofalo *et al* 1999, Jia and Qiu 2003) and suggest that the assumption of constant h may be incorrect during transient CSC. In order to explore the heat-transfer mechanisms during CSC and to provide data at elevated initial substrate temperatures, experiments herein were performed with a Plexiglas® skin phantom coupled with a fast-response thermal sensor.

2. Experimental methods and procedures

2.1. Temperature measurement sensor and surface heating element

The temperature sensor (Aguilar *et al* 2003b, 2003c) consists of a miniature type-K thermocouple (~50 μm bead diameter) placed underneath a thin (20 μm) layer of aluminium foil (10 mm × 10 mm) (figure 1), which is positioned on top of a 30 mm × 30 mm square plate of poly methyl-methacrylate resin (Plexiglas®). The thickness of the plate is 6 mm. Small strips of 50 μm thick cellulose tape (Scotch® tape) are placed between the aluminium foil and the Plexiglas® plate, forming a square box around the thermocouple bead to provide thermal insulation and mechanical support. Thermal paste is applied around the thermocouple bead and between the aluminium foil and the tape to ensure good thermal contact. The purpose

Table 1. Thermal properties and thicknesses of layers used in the temperature sensor. Human skin properties are provided for reference.

Properties	Al foil	Scotch® tape	Plexiglas®	Epidermis	Dermis
Thickness (mm)	0.020	0.050	19	–	–
k (W (m °C)$^{-1}$)	205	0.19–0.25	0.19–0.24	0.34	0.41
ρ (kg m^{-3})	2710	1160–1400	1150–1190	1120	1090
C (J (kg °C)$^{-1}$)	896	1400	1300–1500	3200	3500
α_{avg} (m^2 s^{-1})	844×10^{-7}	1.22×10^{-7}	1.31×10^{-7}	0.95×10^{-7}	1.09×10^{-7}

of this sensor is to provide a skin-like thermal substrate so that the overall heat extraction, Q'', and surface heat flux, q'', are on the same order of magnitude as those expected for human skin. The thin metallic foil coupled with a miniature sensor provides 'real-time' temperature measurement. Since thermal conductivities of Plexiglas® and Scotch® tape are much lower than aluminium, the temperature measurement at the interface ($y = 0$) is likely to be very close to that of the aluminium foil. Published thermal properties of the materials used to build these sensors are shown in table 1, as are those for human skin. The thermal properties of the skin layers are approximated with empirical relations (Takata *et al* 1977) and measured water content of the tissue (Caspers *et al* 2000).

To increase the initial substrate temperature (T_0), a thin flexible heater (KHLV-101/5, Omega Engineering, Stamford, CT) is temporarily placed on top of the aluminium foil. Another K-type thermocouple is attached to the bottom of the skin phantom to obtain the initial temperature distribution. The input voltage to the heater can be adjusted to get the desired initial substrate temperature. Once the temperatures of the top and bottom of the skin phantom become stable, the heater is removed before applying a cryogen spurt to the surface.

All thermocouple measurements are acquired at 2 kHz and converted to temperature data using an A/D converter board and dedicated software (InstruNet™, Omega Engineering, Stamford, CT). This acquisition rate is appropriate because the response time (τ) of the aluminium foil attached to the thermocouple sensor is less than 3 ms. The uncertainty associated with K-type thermocouples used in this study is ± 0.2 °C after calibration.

2.2. Cryogen delivery and nozzle

The cryogen utilized is 1,1,1,2-tetrafluoroethane, also known as R-134a, with saturation temperature $T_{sat} \approx -26.2$ °C at atmospheric pressure. Cryogen is kept in a container at saturation pressure (660 kPa at 25 °C), and delivered through a high-pressure hose to an electronically controlled fuel injector attached to a straight-tube nozzle. The nozzle is made of stainless steel with an inner diameter (d_N) and length (l_N) of 0.7 mm and 63.6 mm, respectively. The nozzle is soldered to a custom-made copper coupling, which in turn fits tightly around the fuel injector. The d_N is similar to that of commercial devices used in laser dermatologic surgery.

2.3. Mathematical model and inverse heat-transfer algorithm

Heat transfer in the skin phantom during CSC is simplified to a one-dimensional heat conduction problem because the diameter of the cryogen spray (∼20 mm) at the phantom surface is much greater than the depth of interest (∼200 μm). Moreover, the temperature distribution does not change significantly in the lateral direction near the centre of the spray

(Franco *et al* 2004). For each layer of substrate, the temperature distribution can be described with the one-dimensional heat conduction equation:

$$\frac{\partial T}{\partial t} = \alpha_i \frac{\partial^2 T}{\partial y^2} \tag{1}$$

where α_i is the corresponding thermal diffusivity of aluminium foil, Scotch® tape and Plexiglas® layer.

Appropriate initial and boundary conditions are needed to solve equation (1). When CSC experiments are performed at room temperature, the phantom temperature is uniform before application of the cryogen spray and thus room temperature is used as the initial condition. When CSC experiments are performed at elevated surface temperatures, e.g., 80 °C, there is a temperature gradient across the phantom because it is heated from the top. However, the temperature difference inside the depth of interest (∼200 μm) is less than 1% of the surface temperature. Therefore, the initial substrate condition can be set to the surface temperature measured by the miniature thermocouple before application of the cryogen spray. Plexiglas® can be treated as a semi-infinite thick body and contact resistances between different layers can be ignored because of the low thermal diffusivity of Plexiglas®, thus, only one boundary condition at the top surface of the aluminium foil is needed:

$$-k_{\mathrm{Al}} \left.\frac{\partial T_{\mathrm{Al}}}{\partial y}\right|_{y=b} = q''(t) \tag{2}$$

where b is the aluminium foil thickness. Because the temperature is measured closest to the point of best thermal contact, i.e., the bottom surface of the aluminium foil, the top surface heat flux $q''(t)$ can be estimated with either an inverse heat conduction (IHC) algorithm or Duhamel's superposition integral by assuming the aluminium foil is isothermal. One of the IHC algorithms, the sequential function specification (SFS) method of Beck *et al* (1985) is employed here. This method is capable of resolving fast transients in surface heat flux and has been used in similar types of experiments to estimate $q''(t)$. Tunnell *et al* (2002) provided a detailed discussion on the accuracy of this method as applied to CSC. Independent of the IHC algorithm, measured temperature data are smoothed by a digital filter (Taler 1996, Aguilar *et al* 2003b) to remove random noise.

Aguilar *et al* (2003b, 2003c) have shown the effect of spurt duration (Δt) and z on CSC when T_0 was room temperature (∼20 °C). They concluded that spurts with Δt longer than 40 ms extract the same amount of heat from the skin within the cooling time ranges used during most clinical applications (10–100 ms). They also found that there are two different CSC regimes as a function of z and the transition between them occurs at $z \approx 25$–30 mm. In this paper, the effect of Δt (20, 50 and 100 ms) and z (50 and 20 mm) on CSC at elevated T_0 was studied first. Thereafter, the effect of T_0 (21, 40 and 80 °C) at two different z were studied.

3. Results

3.1. Effect of Δt for $T_0 = 40$ °C

Figure 2 shows the measured temperatures for three Δt of 20, 50 and 100 ms for $z = 50$ mm and $T_0 = 40$ °C. The measured temperatures drop from 40 to −27 °C after about 45 ms regardless of Δt. Thereafter, the temperatures start to increase slowly for $\Delta t = 50$ and 100 ms irrespective of whether there is cryogen droplets impinging on the surface or not. Cryogen spurt termination does not induce any noticeable change in the temperature curves, which suggests that droplet impingement has a negligible effect on heat transfer between the

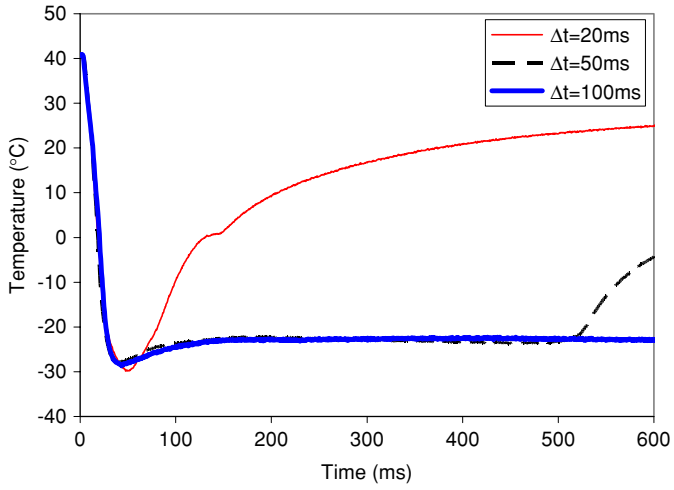

Figure 2. Measured temperature variation as a function of time for $\Delta t = 20$, 50 and 100 ms; $z = 50$ mm, $T_0 = 40$ °C.

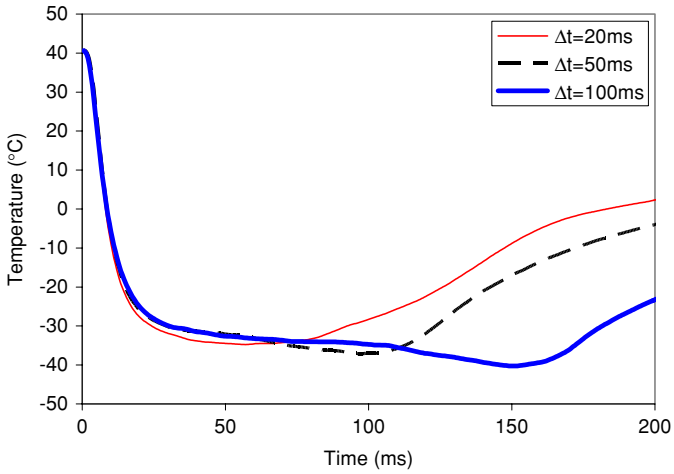

Figure 3. Measured temperature variation as a function of time for $\Delta t = 20$, 50 and 100 ms; $z = 20$ mm, $T_0 = 40$ °C.

cryogen and substrate after a specific period when $z = 50$ mm. Spurts with Δt of 50 and 100 ms produce similar temperature curves, i.e., extract the same amount of heat within the first 100 ms. It can be seen that the effect of Δt on CSC at elevated T_0 is the same as that reported for room temperature by Aguilar *et al* (2003b).

Figure 3 shows the measured temperatures for three Δt of 20, 50 and 100 ms for $z = 20$ mm and $T_0 = 40$ °C. The temperature curves display different trends as compared to those for $z = 50$ mm and the effect of droplet impingement can be seen. The measured temperatures drop from 40 to -30 °C after 30 ms for all three Δt. Thereafter, the temperature remains almost at this value if there is cryogen droplet impingement; otherwise, temperature starts to decrease shortly after spurt termination. The measured temperatures reach their minimum 50 ms after spurt termination and then start to increase. The difference in temperature

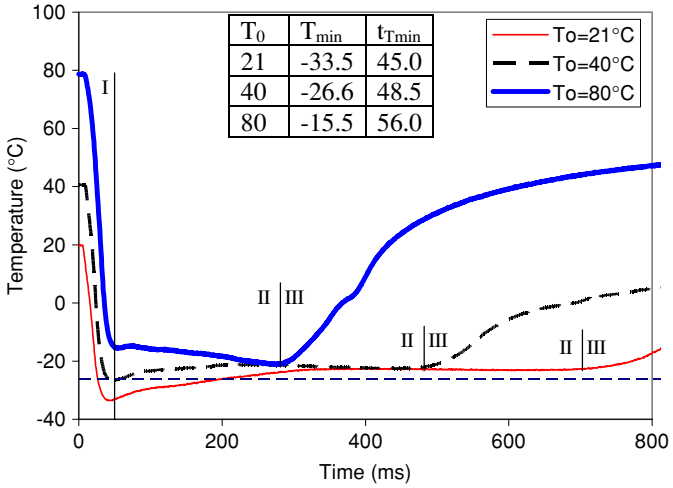

Figure 4. Measured temperature variation as a function of time for $T_0 = 21$, 40 and 80 °C; $\Delta t = 50$ ms, $z = 50$ mm.

curves at $z = 50$ and 20 mm indicates that those two different CSC regimes reported by Aguilar *et al* (2003c) also exist at elevated T_0. Therefore, $z = 50$ and 20 mm are selected to study the effect of T_0 on CSC.

3.2. Effect of T_0 for $z = 50$ mm

CSC experiments at different T_0 for three Δt, 20, 50 and 100 ms were conducted. However, only 50 ms results are shown here because the effect of Δt on CSC heat transfer at different T_0 is similar to that at room temperature. Figure 4 shows the temperature variations as a function of time for $T_0 = 21$, 40 and 80 °C. The temperature curves for different T_0 qualitatively resemble each other. Each can be divided into three regions in terms of their slopes. In Region I, measured temperature decreases sharply from T_0 to a very low temperature, which is defined as the minimum temperature ($T_{\min}$) at a time defined as $t_{T_{\min}}$. In Region II, measured temperatures change slowly. If $T_{\min}$ is equal to or lower than T_{sat} of the cryogen (−26.2 °C, shown as dashed line), measured temperatures increase slowly and stabilize at a few degrees higher than T_{sat}. Otherwise, measured temperatures decrease slowly and stabilize at the same temperature. The time at the end of Region II is defined as the effective cooling time (t_{ec}). In Region III, measured temperatures increase quickly, which indicate the complete evaporation of residual cryogen. It can be seen that T_0 has significant effect on $T_{\min}$ but has only marginal effect on $t_{T_{\min}} \cdot T_0$ has a remarkable influence on t_{ec}, which reduces from 710 ms for $T_0 = 21$ °C to 290 ms for $T_0 = 80$ °C.

Using these data, the surface heat flux (q'') was estimated as a function of time, $q''(t)$ by solving the IHC algorithm. The estimated $q''(t)$ for three different T_0, 21, 40 and 80 °C at $z = 50$ mm are shown in figure 5. For each T_0, $q''(t)$ increases rapidly to a maximum value ($q''_{\max}$) and then drops quickly. $q''_{\max}$ increases with T_0, however, the effect of T_0 on the time needed to reach $q''_{\max}$ is not significant.

Figure 6 shows $h(t)$ corresponding to each of the $q''(t)$ curves in figure 5. The average temperature of the cryogen spray (T_c) to calculate $h(t)$ is −54.4 °C, which can be measured by placing a thermocouple within the spray cone at $z = 50$ mm (Aguilar *et al* 2003a). Although $q''_{\max}$ increases with T_0, $h_{\max}$ is practically the same for different T_0. The $h(t)$ curves for

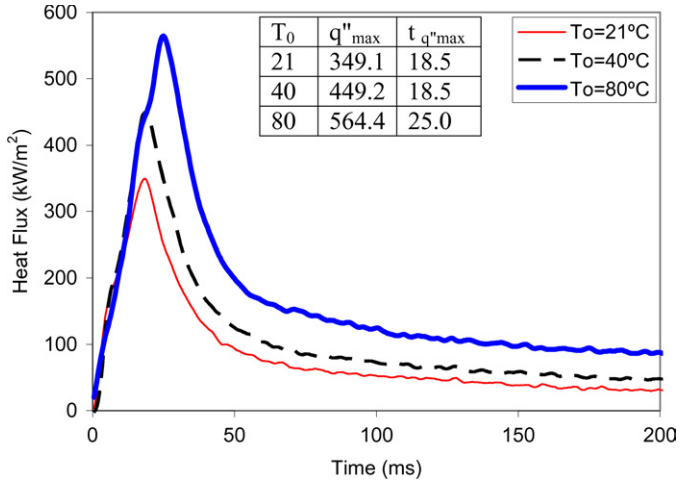

Figure 5. Estimated surface heat flux, q'', as a function of time for $T_0 = 21$, 40 and 80 °C; $\Delta t = 50$ ms, $z = 50$ mm.

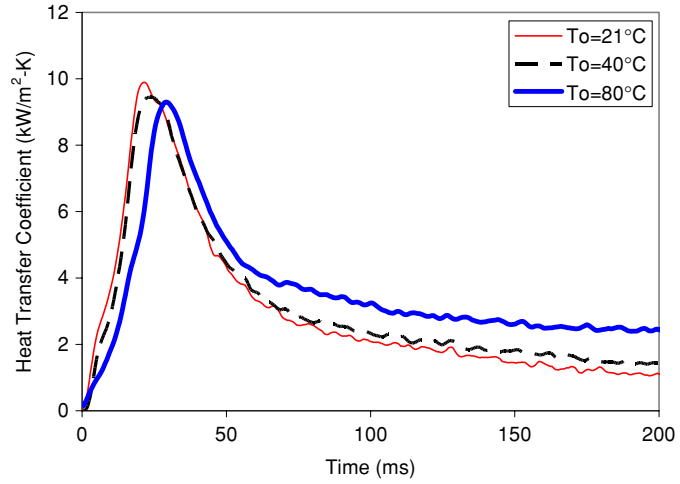

Figure 6. Estimated heat-transfer coefficient, h, as a function of time for $T_0 = 21$, 40 and 80 °C; $\Delta t = 50$ ms, $z = 50$ mm.

$T_0 = 21$ and 40 °C resemble each other. The $h(t)$ curve for $T_0 = 80$ °C has the same shape but it is shifted to the right with a time lag of 5 ms.

3.3. Effect of T_0 for $z = 20$ mm

Figure 7 shows the measured temperature variations as a function of time for $T_0 = 21$, 40 and 80 °C with $z = 20$ mm. The temperature curves can also be qualitatively divided into three regions in terms of their slopes, which are similar to those for $z = 50$ mm. However, unlike $z = 50$ mm, measured temperatures for all three T_0 decrease slowly in Region II and the t_{ec} for different T_0 are similar. Measured temperatures at the end of Region I are -35, -29 and -17 °C for $T_0 = 21$, 40 and 80 °C, respectively. Temperatures continue to decrease to their

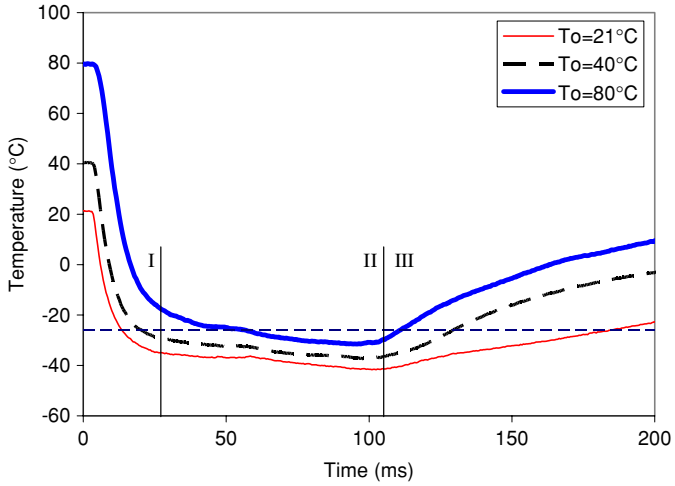

Figure 7. Measured temperature variation as a function of time for $T_0 = 21$, 40 and 80 °C; $\Delta t = 50$ ms, $z = 20$ mm.

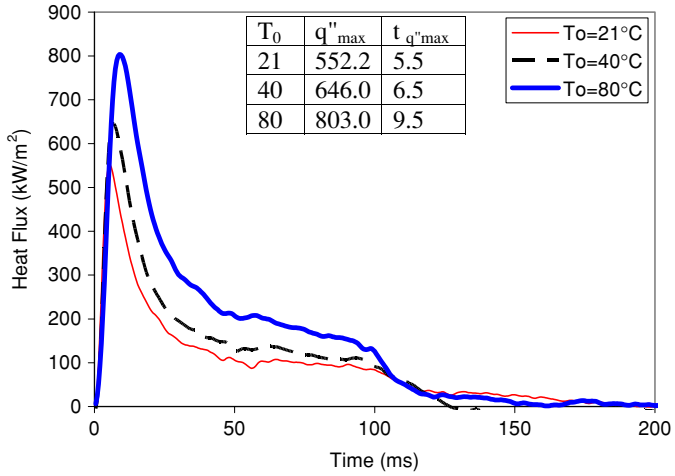

Figure 8. Estimated surface heat flux, q'', as a function of time for $T_0 = 21$, 40 and 80 °C; $\Delta t = 50$ ms, $z = 20$ mm.

minimum until the end of Region II, which are −41, −37 and −31 °C for $T_0 = 21$, 40 and 80 °C, respectively.

The estimated $q''(t)$ for $T_0 = 21$, 40 and 80 °C at $z = 20$ mm are shown in figure 8. The heat-transfer characteristics shown in figure 8 are qualitatively similar to those shown in figure 5 for $z = 50$ mm, with q''_{max} occurring during the spurt and a long slow decrease after spurt termination. For $z = 20$ mm, however, there is a significant increase in q''_{max} for all T_0, compared to that for $z = 50$ mm. In addition, the times needed to reach q''_{max} are also shorter. It can be seen that q''_{max} also increases with T_0 for $z = 20$ mm and the effect of T_0 on the time needed to reach q''_{max} is not significant.

Figure 9 shows the corresponding heat-transfer coefficients, $h(t)$, computed for the same T_0 in figure 8 using the measured value of T_c (−44.6 °C) at $z = 20$ mm (Aguilar *et al* 2003a).

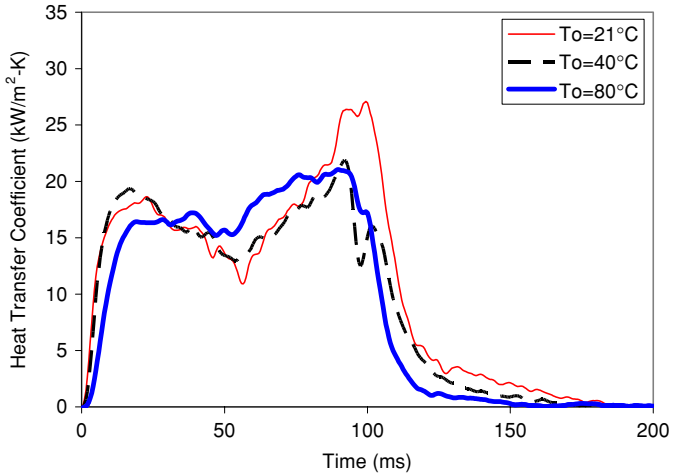

Figure 9. Estimated heat-transfer coefficient, h, as a function of time for $T_0 = 21$, 40 and 80 °C; $\Delta t = 50$ ms, $z = 20$ mm.

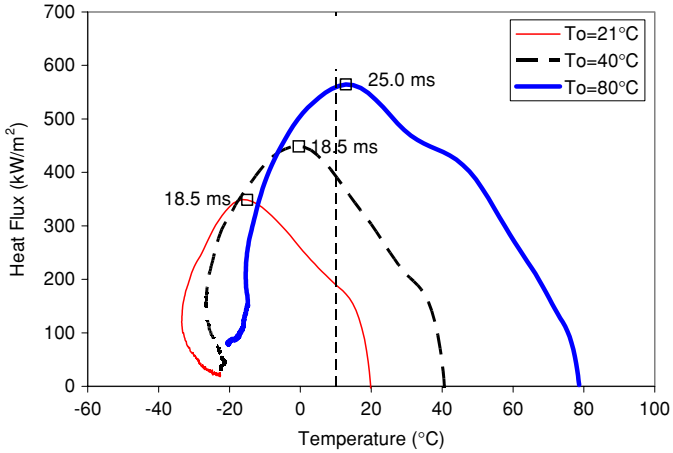

Figure 10. Estimated surface heat flux, q'', as a function of surface temperature for $\Delta t = 50$ ms and $z = 50$ mm.

In agreement with that reported by Aguilar *et al* (2003b) for room temperature, the $h(t)$ curve for $z = 20$ mm is very different to that for $z = 50$ mm. The dynamic variations of h are similar for different T_0. All show a higher average $h(t)$ after a short period of rapid increase, followed by an even higher average $h(t)$ after spurt termination. This behaviour suggests the presence of a very thin liquid layer which evaporates even more efficiently after spurt termination. The existence of this layer, however, is not as noticeable as that resulting from spurts delivered at $z = 50$ mm, and this layer is clearly more unstable as evidenced by the large fluctuations seen in figure 9.

4. Discussion

The heat-transfer mechanisms during CSC may be better understood if q'' is plotted as a function of substrate surface temperature. Figures 10 and 11 show q'' versus surface

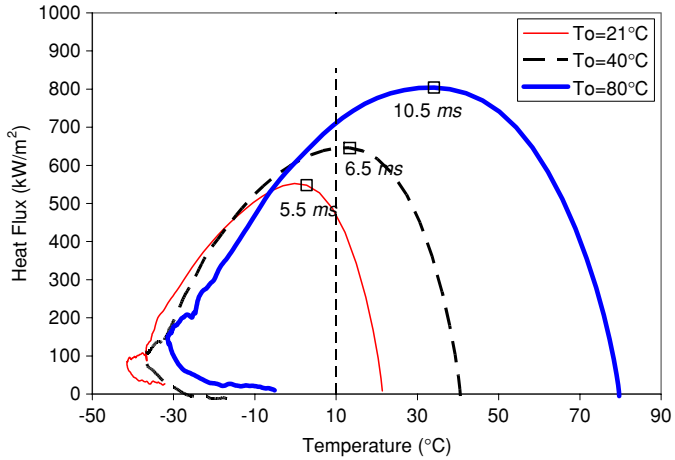

Figure 11. Estimated surface heat flux, q'', as a function of surface temperature for $\Delta t = 50$ ms and $z = 20$ mm.

temperature curves at different T_0 corresponding to $z = 50$ and 20 mm, respectively, both for the same Δt of 50 ms. All curves are qualitatively similar to each other and to those observed for a metal object cooled by a water spray (e.g., Qiao and Chandra 1998, Ciofalo *et al* 1999). However, the transient variation of q'' with surface temperature during CSC cannot be explained by classical boiling theory. For example, when the surface temperature is 10 °C in figures 10 and 11 (shown as vertical dashed lines), the boiling regime for $T_0 = 21$ °C is transition boiling (right of $q''_{\max}$) but it is nucleate boiling (left of $q''_{\max}$) for $T_0 = 80$ °C. Another difficulty when employing classical boiling theory is that the critical surface temperature (i.e., the surface temperature when the heat flux reaches its maximum) changes with T_0. According to classical boiling theory, the critical surface temperature only changes with spray characteristics.

If T_0 is further increased, heat transfer between the cryogen and substrate goes into the film boiling region. Here, the surface is so hot that the momentum of the vapour generated between the cryogen droplets and the hot surface prevents the liquid from wetting the surface. The surface temperature at the beginning of this region is the so-called Leidenfrost temperature (T_{Leid}). Spiegler *et al* (1963) used a Van der Waals equation of state for a liquid to determine T_{Leid}. When the pressure is well below the critical pressure,

$$T_{\text{Leid}} = \frac{27}{32} T_{\text{crit}} \tag{3}$$

where T_{crit} is the critical temperature. Baumeister and Simon (1973) added an empirical factor to equation (3) which accounts for the effect of surface cooling caused by the impingement of a cold droplet:

$$T_{\text{Leid}} = \left(\frac{27}{32} T_{\text{crit}} - T_{\text{L}}\right) \Big/ [\exp(0.0175\beta)\,\text{erfc}(0.042\sqrt{\beta})] + T_{\text{L}} \tag{4}$$

$$\beta = 1/(k\rho C)_{\text{surface}} \ (\text{s cm}^4\ ^\circ\text{C}^2\ \text{cal}^{-2}) \tag{5}$$

where T_{L} is the liquid droplet temperature. For an R-134a droplet with T_{crit} of 101.03 °C and T_{L} of −44.6 °C on an aluminium surface, equation (4) predicts $T_{\text{Leid}} = 50.3$ °C. However, T_{Leid} could be as high as 467.4 °C on a Plexiglas® surface. Although the Plexiglas® skin phantom is covered with aluminium foil, this sensor's T_{Leid} should be somewhere in between

that of aluminium and Plexiglas® but definitely much higher than the highest T_0 in experiments herein because the foil is very thin. Therefore, it is reasonable to assume that heat transfer between the cryogen droplets and skin phantom is still in the nucleate boiling regime (i.e., surface temperature $\ll T_{\text{Leid}}$) even if T_0 is 80 °C. In fact, the heat flux versus surface temperature curves for different T_0 almost merge into one curve after $q''_{\max}$ as shown in figure 11.

Because the surface is dry before cryogen application, it takes a short period of time to completely cover the entire spray area with a thin layer of cryogen. During this period, the surface heat flux can be expressed as

$$q'' = q''_{\text{d}} \frac{A_{\text{d}}}{A} \tag{6}$$

where q''_{d} is the average heat flux for all droplets on the surface, A_{d} is the area covered by these droplets and A is the total spray area. Because heat transfer is in the nucleate boiling region, q''_{d}, decreases with decreasing surface temperature. However, the wetting ratio, $\frac{A_{\text{d}}}{A}$, increases from 0 at the beginning of the spray to 1 after formation of the cryogen film. Because q''_{d} decreases, the heat flux can only increase with the wetting ratio. Once the wetting ratio reaches its maximum, heat flux reaches its maximum. Because the spray is discrete and droplets also rebound and evaporate from the surface, the wetting ratio increases from 0 to 1, i.e., the thin cryogen film forms in a short time period. Correspondingly, an increasing heat flux is observed at the beginning of the cryogen spurt. q''_{d} is higher for higher T_0 when the wetting ratio is 1, which results in higher maximum heat flux for higher T_0.

Because the spray characteristics depend on the nozzle-to-substrate distance, z, the time to form a thin cryogen layer on the surface, i.e., $\frac{A_{\text{d}}}{A} = 1$, should be different for different z, which is observed in our experiments. As shown in figure 10, it required 18.5, 18.5 and 25.0 ms for $T_0 = 21$, 40 and 80 °C, respectively, to form the film (i.e., to reach the maximum heat fluxes as marked by the square symbols) when $z = 50$ mm. For $z = 20$ mm, it required only 5.5, 6.5 and 10.5 ms as shown in figure 11. The short film-forming time for $z = 20$ mm is related to the higher mass flux. The total mass of droplets at $z = 50$ mm is less than that at 20 mm because of in-flight droplet evaporation. The spray area also increases with z (Aguilar *et al* 2001). The long film-forming time for high initial substrate temperature can be explained by more evaporation at higher T_0 which reduces the total cryogen accumulated on the surface. Higher mass flux for $z = 20$ mm and higher droplet velocity also causes higher heat flux (Karapetian *et al* 2003).

From a clinical standpoint, current results are encouraging in terms of improving the therapeutic outcome of laser dermatologic surgery. Skin can be preheated, e.g., 20 °C higher than normal body temperature, using a flexible electrical heater or infrared radiation. Because the maximum heat flux increases with T_0 as shown in figure 12, the epidermis at higher initial temperature can be cooled more effectively than at normal body temperature and the temperature difference between the epidermis and PWS blood vessels is increased. Higher skin temperature may also be helpful to dilate smaller (10–30 μm diameter) PWS vessels, making them more vulnerable to laser irradiation (Svaasand *et al* 2004). Another example of where these results may have clinical utility is in the implementation of multiple-intermittent cryogen spurts and laser pulses combinations, as proposed by Aguilar *et al* (2002). The cooling time of the epidermis, which may have a temperature of 80 °C after the laser pulse, can be shortened because of the high heat flux at this T_0. If the repetition rate of the laser pulses can be matched to this cooling time, the energy absorbed by the PWS vessels can be effectively preserved. It is obvious that clinical conditions are different from those used for the laboratory experiments presented herein as the roughness and thermal diffusivity of normal human skin are different from the current skin phantom. The effect of these parameters on CSC of human skin needs to be further investigated.

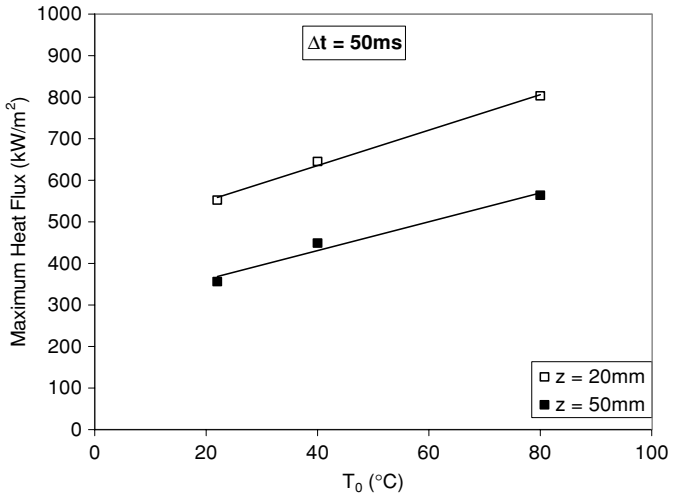

Figure 12. Estimated maximum surface heat flux, q''_{max}, as a function of T_0.

5. Summary and conclusions

Experiments were performed to investigate the effect of the initial substrate temperature (T_0) on the dynamic variation of surface heat flux (q'') and heat-transfer coefficient (h) during CSC. It was found that the maximum heat flux (q''_{max}) increases with increasing T_0 and decreasing nozzle-to-substrate distance (z). T_0 has no significant effect on h. Although the CSC heat flux versus surface temperature curves are qualitatively similar to those observed for a water spray, the transient variations of q'' with surface temperature during CSC cannot be explained by classical boiling theory. It is preferable to assume that heat transfer between cryogen droplets and the skin phantom is still in the nucleate boiling region even if T_0 is 80 °C because T_{Leid} on a Plexiglas® substrate is very high (∼467 °C). Under this assumption, the surface heat flux is determined by the heat transferred into cryogen droplets on the surface and the wetting ratio of the surface. Once the wetting ratio reaches its maximum, heat flux reaches its maximum.

Based on the skin phantom studied, a new preheating scheme is proposed. The skin can be preheated to increase the temperature of PWS blood vessels, while more heat is extracted from the preheated epidermis by a subsequent cryogen spurt. The temperature gradient between the epidermis and PWS blood vessels is increased, which might lead to improved therapeutic outcome.

Acknowledgments

This work was supported by the National Institutes of Health (GM 62177 and AR 47551 to JSN and HD 42057 to GA). Institutional support from the Beckman Laser Institute Endowment is also acknowledged. Laboratory assistance provided by Jie Liu and Henry Vu is greatly appreciated.

References

Aguilar G, Diaz S H, Lavernia E J and Nelson J S 2002 Cryogen spray cooling efficiency: improvement of port wine stain laser therapy through multiple-intermittent cryogen spurts and laser pulses *Lasers Surg. Med.* **31** 27–35

Aguilar G, Majaron B, Karapetian E, Lavernia E J and Nelson J S 2003a Experimental study of cryogen spray properties for application in dermatologic laser surgery *IEEE Trans. Biomed. Eng.* **50** 863–9

Aguilar G, Majaron B, Pope K, Svaasand L O, Lavernia E J and Nelson J S 2001 Influence of nozzle-to-skin distance in cryogen spray cooling for dermatologic laser surgery *Lasers Surg. Med.* **28** 113–20

Aguilar G, Wang G X and Nelson J S 2003b Effect of spurt duration on the heat transfer dynamics during cryogen spray cooling *Phys. Med. Biol.* **48** 2169–81

Aguilar G, Wang G X and Nelson J S 2003c Dynamic behavior of cryogen spray cooling: effects of spurt duration and spray distance *Laser Surg. Med.* **32** 152–9

Anderson R R and Parrish J A 1983 Selective photothermolysis: precise microsurgery by selective absorption of pulsed radiation *Science* **220** 524–7

Baumeister K J and Simon F F 1973 Leidenfrost temperature—its correlation for liquid metals, cryogens, hydrocarbons and water *J. Heat Transfer* **95** 166–73

Beck J V, Blackwell B and St Clair C R 1985 *Inverse Heat Conduction: Ill-Posed Problems* (New York: Wiley)

Caspers P J, Lucassen G W, Bruining H A and Puppels G J 2000 Automated depth-scanning confocal Raman microspectrometer for rapid *in vivo* determination of water concentration profiles in human skin *J. Raman Spectrosc.* **31** 813–8

Chang C J, Anvari B and Nelson J S 1998 Cryogen spray cooling for spatially selective photocoagulation of hemangiomas: a new methodology with preliminary clinical reports *Plast. Reconstr. Surg.* **102** 459–63

Chang C J, Kelly K M and Nelson J S 2001 Cryogen spray cooling and pulsed dye laser treatment of cutaneous hemangiomas *Ann. Plast. Surg.* **46** 577–83

Chang C J and Nelson J S 1999 Cryogen spray cooling and higher fluence pulsed dye laser treatment improve port-wine stain clearance while minimizing epidermal damage *Dermatol. Surg.* **25** 767–72

Ciofalo M, Di Piazza I and Brucato V 1999 Investigation of the cooling of hot walls by liquid water sprays *Int. J. Heat Mass Transfer* **42** 1157–75

Franco W, Wang G X, Nelson J S and Aguilar G 2004 Radial heat transfer dynamics during cryogen spray cooling *Proc. ASME International Mechanical Engineering Congress, IMECE2004-59609 (Anaheim, CA, November 2004)*

Jia W and Qiu H H 2003 Experimental investigation of droplet dynamics and heat transfer in spray cooling *Exp. Therm. Fluid Sci.* **27** 829–38

Karapetian E, Aguilar G, Kimel S, Lavernia E J and Nelson J S 2003 Effects of mass flow rate and droplet velocity on surface heat flux during cryogen spray cooling *Phys. Med. Biol.* **48** N1–6

Kelly K M, Nelson J S, Lask G P, Geronemus R G and Bernstein L J 1999 Cryogen spray cooling in combination with non-ablative laser treatment of facial rhytides *Arch. Dermatol.* **135** 691–4

Nahm W K, Tsoukas M M, Falanga V, Carson P A, Sami N and Touma D J 2002 Preliminary study of fine changes in the duration of dynamic cooling during 755-nm laser hair removal on pain and epidermal damage in patients with skin types III–V *Lasers Surg. Med.* **31** 247–51

Nelson J S, Milner T E, Anvari B, Tanenbaum B S, Kimel S, Svaasand L O and Jacques S L 1995 Dynamic epidermal cooling during pulsed laser treatment of port wine stain—a new methodology with preliminary clinical evaluation *Arch. Dermatol.* **131** 695–700

Nelson J S, Milner T E, Anvari B, Tanenbaum S, Svaasand L O and Kimel S 1996 Dynamic epidermal cooling in conjunction with laser-induced photothermolysis of port wine stain blood vessels *Lasers Surg. Med.* **19** 224–9

Qiao Y M and Chandra S 1998 Spray cooling enhancement by addition of a surfactant *J. Heat Transfer* **120** 92–8

Spiegler P, Hopenfeld J, Silberbeg J, Bumpus C F Jr and Norman A 1963 Onset of stable film boiling and the foam limit *Int. J. Heat Mass Transfer* **6** 987–94

Svaasand L O, Aguilar G, Viator J A, Randeberg L L, Kimel S and Nelson J S 2004 Increase of dermal blood volume fraction reduces the threshold for laser-induced purpura: implications for port wine stain laser treatment *Lasers Surg. Med.* **34** 182–8

Takata A N, Zaneveld L and Richter W 1977 Laser-induced thermal damage in skin *Report* SAM-TR-77-38 US Air Force School of Aerospace Medicine, Brooks Air Force Base, TX

Taler J 1996 Theory of transient experimental techniques for surface heat transfer *Int. J. Heat Mass Transfer* **39** 3733–48

Torres J H, Nelson J S, Tanenbaum B S, Milner T E, Goodman D M and Anvari B 1999 Estimation of internal skin temperatures in response to cryogen spray cooling: implications for laser therapy of port wine stains *IEEE J. Sel. Top. Quantum Electron.* **5** 1058–66

Tunnell J W, Torres J H and Anvari B 2002 Methodology for estimation of time-dependent surface heat flux due to cryogen spray cooling *Ann. Biomed. Eng.* **30** 19–33

Waldorf H A, Alster T S, McMillan K, Kauvar A N, Geronemus R G and Nelson J S 1997 Effect of dynamic cooling on 585-nm pulsed dye laser treatment of port-wine stain birthmarks *Dermatol. Surg.* **23** 657–62